Time reversal of RF signals via cascaded time-to-frequency and frequency-to-time mapping in frequency-shifting loops

Guénolé Dandé, Vincent Billault, Jérôme Bourderionnet, Hugues Guillet de Chatellus

Research Article | Vol. 33, No. 14 / 14 Jul 2025 / Optics Express 30316
Optics EXPRESS

Time reversal of RF signals via cascaded time-to-frequency and frequency-to-time mapping in frequency-shifting loops

GUÉNOLÉ DANDÉ,[1,2] VINCENT BILLAULT,[2] JÉRÔME BOURDERIONNET,[2] AND HUGUES GUILLET DE CHATELLUS[1,*]

[1] Univ Rennes, CNRS, Institut FOTON - UMR 6082, 35000 Rennes, France
[2] Thales Research and Technology France, 91767 Palaiseau, France
[*] hugues.guilletdechatellus@univ-rennes.fr

Abstract: Time reversal of radio-frequency or microwave signals has important applications applications in telecommunications and electronic warfare. All-digital techniques are intrinsically limited in bandwidth by the speed of the converters, which necessitate the emergence of alternative analog techniques for future implementations. We demonstrate a new, to our knowledge, microwave-photonics architecture in this context, offering integration prospects. The system we propose is based on a pair of frequency-shifting loops, where the first loop transfers the input signal from the time domain into the frequency domain. In contrast, the second loop performs the opposite process, thus achieving the desired time-reversal process. The technique is particularly versatile, allowing the time reversal of signals with bandwidths of the order of tens of MHz, durations on the order of tens of microseconds, and with arbitrarily small latency. The system can also act as a temporal buffer for the reversed signal, a promising feature for photonic-based beamforming.

1. Introduction

Time reversal is a concept that was initially studied and demonstrated in the field of acoustic waves, for focusing ultrasonic waves through heterogeneous media [1]. The idea behind time reversal is as follows: a source placed in an enclosure emits a pulse. Transceivers located on the surface of the enclosure record the signals received. If these transceivers in turn synchronously retransmit a reversed version of the recorded signal, the sum of the signals will produce a pulse at the position of the source [2]. This concept of a time-reversal cavity can be generalized when the signal is not collected at all point of the enclosure, but on a fraction of it (time-reversal mirror). The technique can even be generalized to single-transceiver configurations, in particular configurations, such as reverberant cavities, or highly diffusing media. Under these conditions, the signal returned by a single transceiver returns to focus at the position of the source point. From a practical point of view, these concepts have found applications in medicine [3,4], underwater communications [5–7], and seismology [8]. The generalization of this concept to the case of electromagnetic waves opens up many possibilities of application, particularly for communications in complex environments (scattering, diffraction, reflection) [9–13]. Additionally, the possibility of sending a signal in a spatially and temporally targeted manner makes it possible to envisage intentional electromagnetic interference systems, or the neutralization of transmitters.

On a practical point of view, time reversal can readily be achieved by digital sampling of the received signal, numerical reversal, and digital-to-analog conversion. This all-digital approach is adapted to signals with bandwidths up to a few tens to a few hundreds of MHz. However, for faster signals, digital techniques become complex to implement because of the bottleneck of the ADC and DAC performance beyond a few GSa/s. In this context, it is important to develop information processing technologies that no longer rely on the digital paradigm, but

#564275 https://doi.org/10.1364/OE.564275
Journal © 2025 Received 3 Apr 2025; revised 22 May 2025; accepted 29 May 2025; published 10 Jul 2025

Optics EXPRESS

enable fast signals to be processed on the fly, without excessive energy consumption. Analog approaches have demonstrated increased interest in recent years [14]. Many of these are based on photonics, which a priori offers many advantages: the extreme potential bandwidth, the insensitivity to electromagnetic disturbances, the potential for integration, and low-loss propagation, which guarantee prospects for energy-efficient practical implementations. So far, most of photonics-based approaches of time reversal are derived from the space time analogy, which provides the time-domain equivalent of imaging systems [15]. More precisely, a quadratic temporal phase modulation realizes a time lens, while the propagation through a dispersive medium is the equivalent of the propagation of optical wavefronts through the free space. Several implementations have been reported so far and have proven successful for signals with duration in the ns range [16–19]. However technical limits including the duration of time lenses and the amount of dispersion available in optical components prevent the use of optical methods for time reversal of longer signals that would be suited for real-world applications. To overcome this limitation and return signals with durations exceeding the μs, an original alternative has been developed, based on the use of a three-pulse photon echo sequence in a rare-earth ion-doped matrix [20–22]. However, the latency time exceeds the 100 μs range and overall, this approach, which requires cryogenic conditions and the use of a frequency-swept laser source, remains complex to implement.

In this paper, we present a new an simple technique based on photonics, which makes it possible to get rid of the limits posed by temporal optics. We show that an original architecture based on two cascaded frequency shifting loops (FSL) [23] can reverse signals with durations of up to several tens of μs, and with a latency time that can be arbitrarily small. Our concept also makes it possible to store the returned signal on demand before re-transmitting it, a crucial feature for synchronized signal retransmission such as beamforming. The proof-of-principle reported here offers great flexibility, wide prospect for improvement, and can be generalized to many types of signal, depending on the intended application.

2. Concept and experimental set-up

2.1. Principles of the experiment

In broad terms, the concept we propose, depicted in Fig. 1, essentially comprises two steps. The first one consists of a time-to-frequency mapping of the input signal in a first FSL, and of a signal extraction using a time gate. This combination provides a waveform, whose spectral profile reproduces in frequency that of the input signal. The second step consists in sending this waveform to a second loop with a frequency shift opposite to the first one, at the output of which is placed a detector followed by a frequency filter. This second step enables the signal to be projected back from the spectral domain into the temporal domain (frequency-to-time mapping), thus performing the time reversal of the original signal.

2.2. Experimental setup

The basic building block of the system is a frequency shifting loop (FSL), i.e. a fiber loop containing an acousto-optic frequency shifter (AOFS). The FSL also comprises an optical amplifier to compensate for the intrinsic losses of the loop, and an optical bandpass filter (TBPF). The role of the latter is to limit the influence of the amplifier's spontaneous emission (ASE) of the amplifier, and to control the number of roundtrips of the light in the FSL. As such, when seeded with a single frequency laser, the FSL is a simple and compact source of frequency combs and has proven many applications for spectroscopy, generation of linearly frequency modulated waveforms or remote sensing [24–26]. The FSL can also be seeded by a CW laser (amplitude: E_0,

Optics EXPRESS

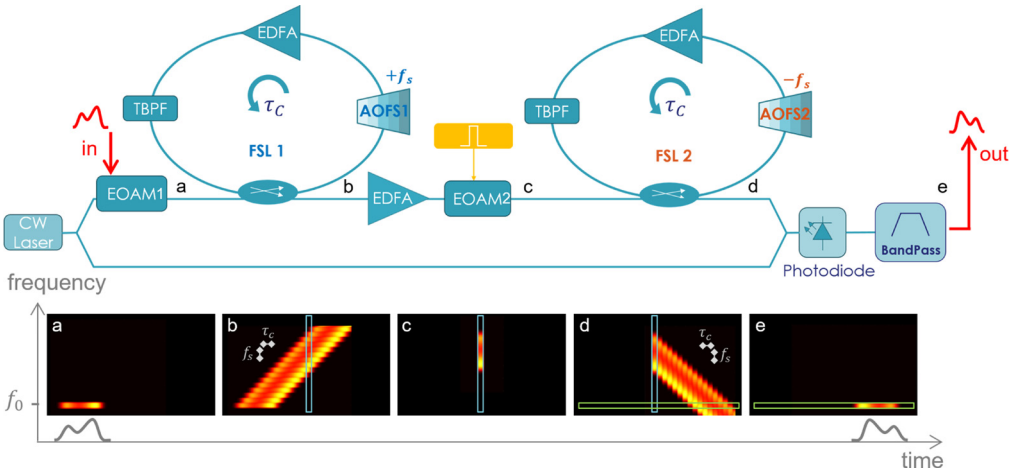

Fig. 1. Operation principle of the time reversal concept. Top : the system consists of two frequency shifting loops (FSL) in cascade, seeded by a CW laser modulated in amplitude by the RF signal of interest (EOAM 1). Both FSL comprise an optical amplifier (EDFA), and an optical bandpass filter (TBPF). The travel times in the FSL are identical (equal to τ_c), and the frequency shifts (f_{s1} and f_{s2}) are respectively equal to +80 and −80 MHz. An EDFA and a time gate (EOAM 2) are placed between FSL 1 and FSL 2. At the FSL 2 output, the optical signal is recombined with the seed laser on a photodiode. The electrical signal is filtered by a low pass filter (40 MHz cut-off frequency). Bottom : representation in the time-frequency plane, of the optical signals at different positions (a to e) in the above set-up. The time gate is represented by the vertical rectangle (in positions b, c, d), while the frequency gate is depicted by the horizontal rectangle (in positions d and e) - see text.

frequency: f_0) modulated by a RF signal of interest $s(t)$. In this case, the output field writes [27]:

$$E(t) = E_0 \sum_{n=0}^{N} s(t - n\tau_c) e^{i2\pi(f_0 + nf_s t)} e^{i\phi_n}, \tag{1}$$

where τ_c is the travel time in the loop, f_s is the frequency shift per roundtrip, and $\phi_n = 2\pi n f_0 \tau_c + \pi n(n+1) f_s \tau_c$. Then, the optical field at the FSL output consists of replicas of the input signal - mapped into the optical domain - shifted both along the time, and the frequency domain, respectively by τ_c and by f_s. Recall that this formal expression is at the origin of numerous microwave-photonics applications of the system [23,28–31].

Here, the architecture consists of two FSL (FSL 1 and FSL 2) in cascade (Fig. 1, top). The AOFS in FSL 1 and FSL 2 are respectively labeled by AOFS 1 and AOFS 2. They are both driven at 80 MHz, but AOFS 1 provides a positive frequency shift (f_{s1} = +80 MHz), while AOFS 2 provides a negative one (f_{s2} = −80 MHz). The travel times in the two loops are both equal to τ_c = 143.0 +/- 0.5 ns. FSL 1 is seeded by a single frequency laser modulated in amplitude by $s(t)$, the electrical signal to be reversed (EOAM 1). The latter is provided by means of an arbitrary waveform generator (AWG). To avoid recirculation of the ASE in FSL 1 prior tho the injection of the signal, the voltage driving AOFS 1 is triggered by the beginning of $s(t)$.

After the amplitude modulator, at the input of FSL 1 (position a in Fig. 1), the optical field consists of a carrier at frequency f_0 modulated by an envelope $s(t)$. At the output of FSL 1 (position b), the optical signal consists of the sum of replicas of $s(t)$, shifted along time and frequency (respectively, by multiples of τ_c and f_{s1}). Then, the signal is amplified in an EDFA prior to a time gate. The latter is achieved by means of an intensity modulator (EOAM 2), driven by a control signal. The modulator is biased to zero. In the absence of an electrical signal, it

Optics EXPRESS

behaves like a closed gate. The control signal is an electrical pulse with a duration set equal to τ_c, and an amplitude equal to the V_π of the modulator. The modulator therefore behaves like a open gate at the moment of the pulse. The frequency content of the optical signal selected by the time gate (position c) therefore reproduces the time dependency of the $s(t)$, thus performing time-to-frequency mapping of the input signal. Note that the tail of the input signal, which has completed fewer turns in FSL 1, is projected at lower frequencies than its head.

The signal then enters FSL 2. Similarly, the RF signal driving AOFS 2 is triggered by the time gate, to prevent ASE from circulating in FSL 2 prior to the signal injection. The signal in FSL 2 then performs a number of turns, during which its carrier frequency is decreased by 80 MHz per turn (position d). At the output of FSL 2, the optical output signal is recombined with a fraction of the injection laser on a balanced detector, thus converting optical frequencies to radio frequencies. An electrical low-pass filter (cut-off frequency: 40 MHz) is then used to convert the frequencies of the output signal to time. The filter plays the role of a frequency gate (i.e. the counterpart in the spectral domain, of the time gate placed at the output of FSL 1). Since the tail of the input signal was projected at a lower frequency after the time gate, it emerges first from the detection signal, thus performing the time reversal of the input signal (position e). Finally, the recombination of the optical signal at the output of FSL 2 with the injection laser on the balanced detector provides one of the two quadratures of the output signal. The modulus of the detection signal (i.e. the reversed version of $s(t)$), is then obtained by an Hilbert transform performed offline.

In practice, and in order to limit the number of components, the two FSL are implemented in a single bidirectional architecture, in which the two directions of circulation see different frequency shifts [32]. For this purpose, a system of two circulators is used to route the signal travelling in one direction to one frequency shifter, and the signal travelling in the other direction to the other frequency shifter. Thus, the bidirectional FSL constains a single TBPF and a single EDFA, both bidirectional. To inject the signal leaving FSL 1 into FSL 2, a Faraday mirror is placed just after the time gate.

3. Experimental results

3.1. Impulse response of the system

In a first set of experiments, we characterize the impulse response of the system, i.e. its capability to store an input elementary pulse by successive positive and negative frequency shifts, and to retransmit it on demand.

To this end, we modulate the injection laser with a pulsed signal of 100 ns duration, i.e. slightly less than τ_c. Here, the time gate between FSL 1 and FSL 2 is kept open, so that the signal can be measured during its whole storage phase in the two FSL. The role of the time gate here is governed by the signals driving the AOFS. First, AOFS 1 is powered on by an RF waveform at 80 MHz, while AOFS 2 is off. The signal travels repeatedly in FSL 1, being shifted in frequency with each turn. A fraction of the recirculating signal is continuously picked up by the output coupler, then injected and extracted from FSL 2 without having completed a turn (since AOFS 2 is not powered). The signal is then recombined with the injection laser, and detected by a fast photodiode. A Fourier transform oscilloscope (11 GHz analog bandwidth) is used to compute the windowed Fourier transform of the photodetection signal. The complete time trace of the detection signal is shown in Fig. 2(a). The first microseconds (Fig. 2(b)) show the first seven signal replicas, whose frequency increases by 80 MHz each time. After a duration corresponding to 46 roundtrips in FSL 1, AOFS 2 is then powered on. For a duration of τ_c, both AOFS are powered simultaneously, then AOFS 1 is switched off. This selects the replica of the input signal that has completed 47 turns in the first loop, and feeds it back into FSL 2, where its frequency is reduced in 80 MHz steps. The output coupler in FSL 2 extracts a fraction of the signal. The end of the temporal trace is plotted in Fig. 2(c), and shows the replicas of the signal during the final

Optics EXPRESS

stages of its descent in frequency towards DC. The spectrogram of the complete trace is plotted in Fig. 2(d), showing clearly the rise and fall in frequency in discrete 80 MHz steps over the whole sequence. These results also emphasize that the signal storage time in the system is equal to the duration of frequency ramps, and can be easily controlled by the timing of the time gate.

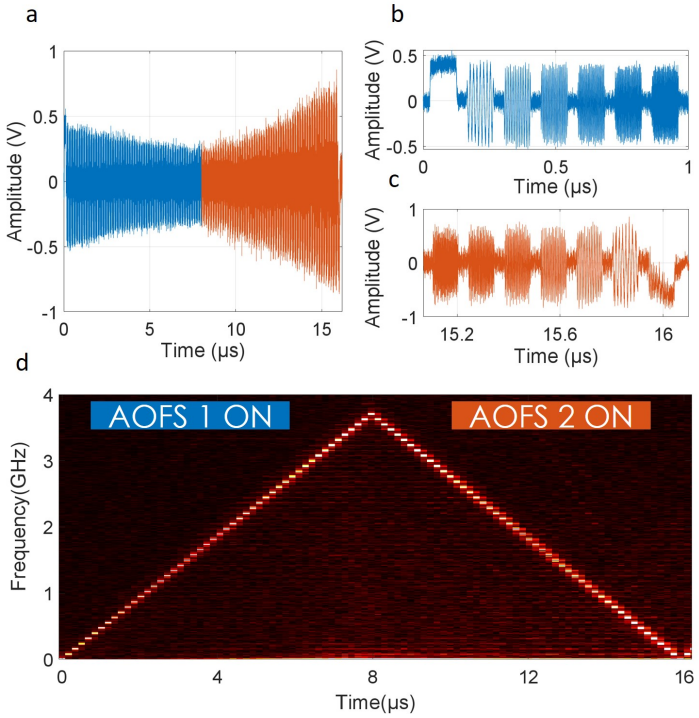

Fig. 2. a : Temporal trace measured by a fast photodiode at the system output. The temporal gate is kept open (see text). b : Zoom of the temporal trace at short times, showing the first frequency shifted replicas of the input signal. c: Temporal trace at the end of the signal frequency downshift sequence. d : Experimental spectrogram of the whole temporal trace obtained by a windowed Fourier transform.

This experiment is also useful for calibrating the system's response. The time trace in Fig. 2(a) shows a slight decrease in the signal amplitude during the upward phase in FSL 1, followed by a slight increase during the downward phase in FSL 2. This is due to the specific gain dynamics of the EDFA [33]. Measuring this signal variation as a function of the number of turns provides a calibration of the system response, which can be applied to the time reversal experiments described next. More precisely, this calibration consists of dividing the amplitude of the reversed signal by the (slightly increasing) envelope profile of the signal amplitude in Fig. 2(a). Additionally, in the next experiments, to avoid biases related to Hilbert transformation of baseband signals, we choose slightly different values of the AOFS frequencies (80.00 MHz and 80.10 MHz typically), so that the signal at the end of the down frequency sequence is not exactly DC, but exhibits oscillations, for more accurate envelope detection.

3.2. *Experimental time reversal of pulsed signals*

In a second set of experiments, we demonstrate the system's ability to reverse pulsed signals. First, the injection laser is modulated with a 56-bit binary signal. Each bit has a duration slightly lower than τ_c. The total duration of the input signal is therefore 8 μs ($56 \times \tau_c$). The time gate

Optics EXPRESS

is applied at 9 μs after the beginning of the sequence. Figure 3(a) shows the input signal, and Fig. 3(b) the raw output trace. Then, we compare the modulus of the Hilbert transform without (Fig. 3(d)), and with (Fig. 3(e)) compensation by the system's response, with the expected reversed signal (Fig. 3(c)). The storage time here is about 2 μs.

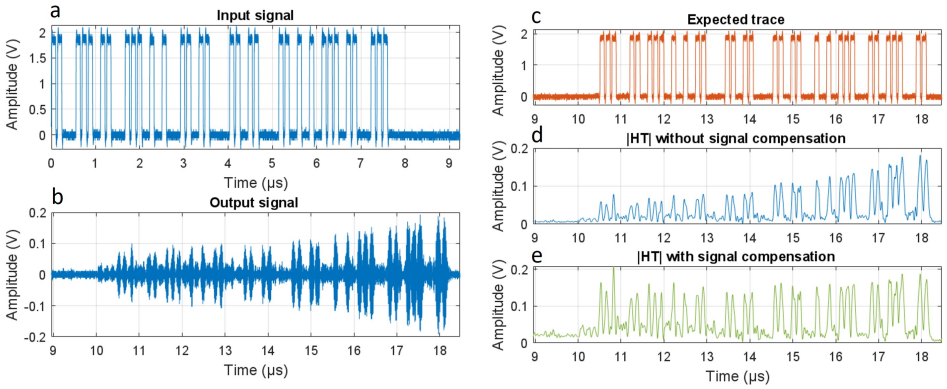

Fig. 3. Experimental time reversal of a 56 bits binary signal. The input sequence is made by the ASCII code of the word " sseccus" (reverse of "success"). a: Input signal. b: Raw output trace. c : Expected trace. d (resp. e): Modulus of the Hilbert transform of the output signal without (resp. with) signal compensation.

Second, we demonstrate the technique's ability to reverse signals whose information is coded in amplitude. To do this, a signal whose envelope represents the profile of a truck is sent into the loop. Figure 4 compares the experimentally returned signal (after Hilbert transform and compensation by the system's response function) with the expected signal. Here again, there is excellent agreement between the two, illustrating the system's ability to reverse a given signal with a high degree of fidelity.

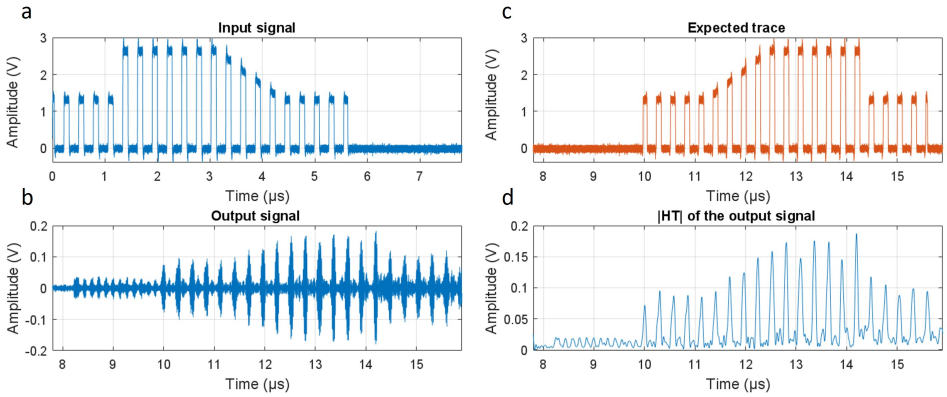

Fig. 4. Experimental time reversal of an input signal modulated in amplitude. The input sequence maps the profile of a truck. a: Input signal. b: Raw output trace. c : Modulus of the Hilbert transform of the output signal without, and with signal compensation (in blue and green respectively). The expected trace is plotted in red.

Optics EXPRESS

3.3. Experimental time reversal of continuous signals

Here we demonstrate the architecture's ability to reverse continuous signals. This is a particularly important issue, especially for spatio-temporal focusing of radio signals. We consider a typical case study, where a given signal (a short radio pulse) passes through a filter. The transmitted signal corresponds to the convolution product of the filter impulse response and the initial pulse. Then, sending the temporally reversed signal back through the same filter should result in the output being the original short pulse. To tackle this problem, we use an electrical pulse of about 100 ns. Several analog low-pass filter models with different cut-off frequencies are tested. The left column of Fig. 5 shows the modulus of the electrical signals after filtering, at the modulator input. The right column shows the modulus of the signal at the output. The latter is obtained by computing the modulus of the Hilbert transform. The filter cut-off frequencies are 2.5 MHz, 1.9 MHz, 1 MHz and 500 kHz respectively, from top to bottom. The reversed traces reproduce the input signals fairly faithfully. Notice that a discretization appears on the output traces, resulting in a stair-step profile (Fig. 5, a.2 to d.2). This phenomenon is due to the time-reversal process itself, where the time gate between the two loops (duration $\approx \tau_c = 143$ ns) dictates the discrete nature of the output signal. Ideally, the time gate should have a flat-top profile, with a duration of exactly τ_c. If the duration of the window is greater, interference effects are observed between two successive bins of the returned signal. On the other hand, if the window duration is less than τ_c, the output signal resembles a pulse train, similar to what is obtained in the case of pulsed signals. In practice, because of the rise and fall time (2 ns) of the pulse generator used to create the time gate, we use a time gate slightly shorter than τ_c, which results in brief signal cancellations at the period of τ_c (Fig. 5, a.2 to d.2). The lower part of Fig. 5 shows the same traces as above, but in logarithmic scale. These results show that the time reversal process only slightly degrades the noise floor of the signal.

Then, we investigate the possibility of accessing the negative components of the reversed signal. Given that the technique is intrinsically coherent, it is theoretically possible to reverse signals with negative components, or even complex signals. To illustrate this capability (Fig. 6), we plot in red (top trace) the raw detection signal, in the case where the input signal is an electrical pulse (100 ns duration) after passing through a low-pass filter (cut-off frequency: 1 MHz). In navy blue, we represent the envelope of the raw signal, determined by calculating its Hilbert transform. Notice the discretization effect induced by the time gate described above. We compare this envelope with the real signal applied to the modulator, and with its opposite (in blue). The lower trace shows the instantaneous phase of the signal (in green). This phase is obtained by calculating the phase of the Hilbert transform, and subtracting a linear phase term, which corresponds to the oscillation of the raw trace (Recall that the offset frequencies in the two loops do not compensate each other exactly, so that the detection of the output signal is not done at DC.) We notice that the phase is constant in the main lobe (i.e. between 6.7 and 7.5 μs). On the other hand, the phase experiences a jump at the level of the first secondary lobe (between 6.3 and 6.7 μs). This phase jump (theoretically equal to π) corresponds to the fact that the amplitude at the level of this lobe becomes negative. The noise level is then too high to detect phase jumps corresponding to the next secondary lobes.

3.4. Control of the emission timing of the reversed signal

In a last set of experiments, we prove the system's ability to control the retransmission time of the reversed signal. As said, this can be done simply by controlling the timing of the time gate relative to that of the input signal. If the time gate is applied just after the input signal has entered the loop, then the beginning of the returned signal (i.e. the end of the input signal) is immediately detected at the output. This means that the latency time can be arbitrarily small, depending only on the fiber length between the input modulator and the photodiode. In the general case, defining t_f as the time where the end of the input signal enters in the loop, and t_g as the timing of the

Optics EXPRESS

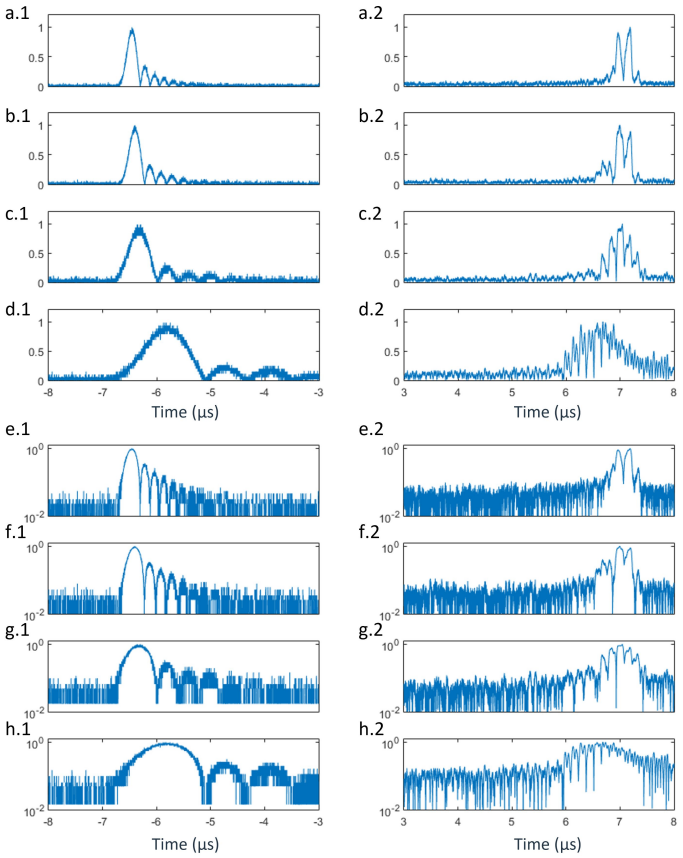

Fig. 5. Left column: modulus of the input RF signal as a function of time. Right column: modulus of the Hilbert transform of the output signal. The input signals are obtained by filtering a 100 ns long electrical pulse by low pass filters having different cutoff frequencies (a: 2.5 MHz, b: 1.9 MHz, c: 1 MHz, and d: 500 kHz). Plots e to h correspond to the cases a to d respectively, displayed in a logarithmic vertical scale.

time gate, the total storage time is simply $2(t_g - t_f)$. The maximum value of this storage time depends on the maximum number of turns that the signal can make in the loop. To demonstrate the flexibility of the storage, we send an 8-bit binary signal (10110111) into the loop and measure the system's output signal for different timings of the time gate. The results plotted in Fig. 7, show the capability of triggering the emission time of the reversed signal simply by controlling the timing of the time gate. Here, the storage time of the signal in the system can exceed 10 μs.

Optics EXPRESS

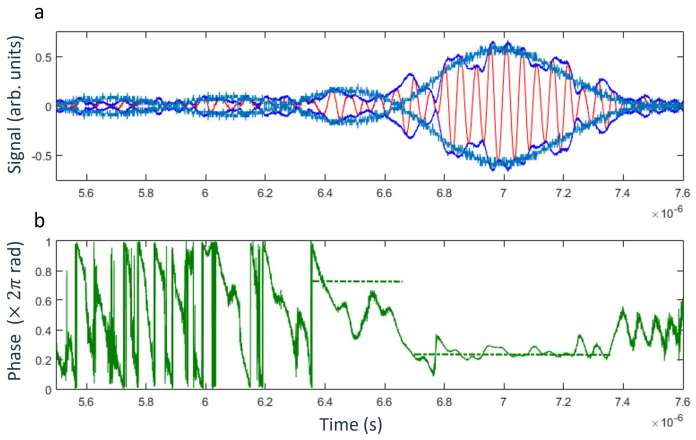

Fig. 6. a: Comparison of the experimental reversed trace (raw signal in red, envelope in navy blue) with the expected envelope (blue). The envelope of the experimental signal is obtained by Hilbert transform of the raw signal. b: Experimental phase obtained by the Hilbert transform of the raw output signal. The dotted lines are indicative phase levels. One (right) corresponds to the average phase in the main lobe, the other (left) would correspond to the phase of the first secondary lobe, shifted by π with respect to the one of the main lobe.

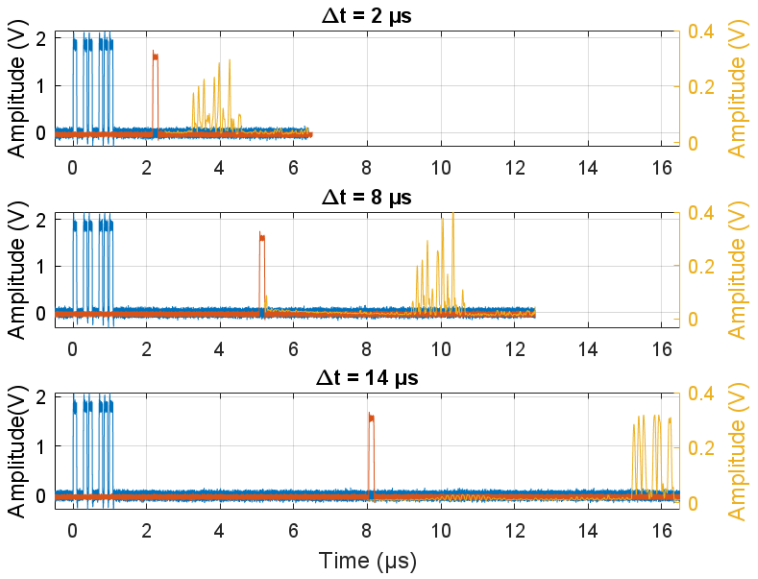

Fig. 7. Timing sequences of time reversal obtained for different timings of the time gate. The binary input signal is plotted in blue. The modulus of the Hilbert transform of the output signal is in yellow. The time gate (in red) is varied, so as to provide delays between the trailing edge of the input signal and the leading edge of the output reversed signal between 2 and 14 μs (from top to bottom).

Optics EXPRESS

4. Discussion and conclusion

We have established the proof of principle of a new, purely photonic technique for time-reversal of both pulsed and continuous RF signals. The technique is simple and relies on commercial telecom components, while offering prospects for integration. It is intrinsically coherent, enabling to reverse signals with positive and negative values, and even complex signals. The storage time of the signal can be controlled electrically. The minimum storage time (i.e. the latency time of the reversal process) can be set arbitrarily small. Unlike conventional microwave photonic approaches, it enables the processing of signals of several tens of μs duration, and tens of MHz bandwidth suggesting future real-world applications (telecommunications, electronic warfare...).

In Table 1, we compare the performance of the technique with previously reported results. Our results are comparable to those of more complex techniques [22]. Moreover, in addition to its simplicity, its intrinsic coherence and potential for integration, our technique offers numerous prospects for improvement to envisage more demanding applications.

Table 1. Performance comparison table for the main time reversal techniques. The Bandwidth column gives the maximum bandwidth value demonstrated experimentally. The Signal duration column indicates the maximum duration of reversed signals. The Coherent column specifies whether the technique can reverse signals with negative or complex values. The Integration column indicates the technique's potential for photonic integration.

Ref.	Platform	Bandwidth	Signal duration	Coherent	Integration
[16]	Photonic	12 GHz	2 ns	no	no
[9]	Electronic	2 MHz	10 μs	yes	
[14]	Electronic	5 MHz	2 ns	yes	
[18]	Photonic	4 GHz	10 ns	no	yes
[19]	Photonic	2.4 GHz	2 ns	no	yes
[22]	Rare-earth doped crystal	50 MHz	12 μs	yes	no
This work	Photonic	10 MHz	10 μs	yes	yes

First, the maximum bandwidth of the input signals is equal to $1/\tau_c$, i.e. about 10 MHz. To increase this value, we need first to reduce the fiber length of the FSLs, which could lead to bandwidths of the order of a hundred MHz. To increase this value still further, fiber architectures should be replaced with integrated ones, which may offer interesting prospects for compact, high-performance systems for processing multi-GHz bandwidth signals. A second condition for increasing the signal bandwidth is to reduce accordingly the duration of the time gate. The latter has a duration set close to τ_c - i.e. close to 140 ns here -, a value that could be substantially reduced.

In the current configuration, a digital Hilbert transform is used to access the envelope of the output signal. This adds a digital processing step to the output signal. This operation could be carried out in an analog fashion, using optical coherent detection, which would provide the two quadratures of the output signal.

The time-bandwidth product (TBWP) can be defined as the product of the signal duration by its bandwidth. Equivalently, it is equal to the number of roundtrips that the signal can achieve in the FSL. Here, we have reported a value of the TBWP equal to 56. In practice, the maximum number of turns (i.e. the maximum TBWP) can exceed 300 [25], which would lead to the possibility of reversing signals with durations exceeding 30 μs. Ultimately, the maximum number of roundtrips is limited by the ASE of the amplifier placed in the FSL, which accumulates with every turn in the loop. The influence of ASE can be quantified using simple models [34,35].

The concept of time reversal reported here can also be adapted to more general concepts of signal processing. In the present configuration where $f_{s1} = -f_{s2}$, the output signal is the reverse

Optics EXPRESS

of the input signal. In the general case, the output signal is a scaled version of the reversed input one and is equal to $s\left(\frac{f_{s2}}{f_{s1}}t\right)$. Therefore adjusting the values of f_{s1} and f_{s2} gives the possibility of controlling the temporal magnification of the output signal.

Finally, the we have demonstrated a storage time of 14 μs. Assuming that 300 round trips in the loop are possible [25], we can therefore consider that, for loops with travel times of a hundred ns, delays of up to 60 μs are possible ($2 \times 300 \times \tau_c$). The system's ability to control the storage time of a signal before sending back its reversed version is a crucial advantage for beamforming techniques, as it enables true time delays to be produced on demand. We expect that in the future, the combination of the concept developed here with the perspective of integrated architectures might find important applications in phased array antennas for communications networks.

Funding. Association Nationale de la Recherche et de la Technologie; Centre National de la Recherche Scientifique (Prematuration 2021); Région Bretagne (CPER PhotBreizh); Rennes Metropole (AIS 2024); FEDER (CPER PhotBreizh); Rennes Metropole (CPER PhotBreizh).

Disclosures. The authors declare no conflicts of interest.

Data availability. Data underlying the results presented in this paper may be obtained from the authors upon request.

References

1. M. Fink, "Time reversed acoustics," Phys. Today **50**(3), 34–40 (1997).
2. B. E. Anderson, M. Griffa, C. Larmat, *et al.*, "Time Reversal," Acoust. Today **4**(1), 5–16 (2008).
3. M. Fink, G. Montaldo, and M. Tanter, "Time-reversal acoustics in biomedical engineering," Ann. Rev. Biomed. Eng. **5**(1), 465–497 (2003).
4. M. Pernot, J.-F. Aubry, M. Tanter, *et al.*, "In vivo transcranial brain surgery with an ultrasonic time reversal mirror," J. Neurosurg. **106**(6), 1061–1066 (2007).
5. R. D. Jackson and D. R. Dowling, "Phase conjugation in underwater acoustics," J. Acoust. Soc. Am. **89**(1), 171–181 (1991).
6. G. F. Edelmann, T. Akal, W. S. Hodgkiss, *et al.*, "An initial demonstration of underwater acoustic communications using time reversal," IEEE J. Ocean Eng. **27**(3), 602–609 (2002).
7. C. Prada, J. de Rosny, D. Clorennec, *et al.*, "Experimental detection and focusing in shallow water by decomposition of the time reversal operator," J. Acoust. Soc. Am. **122**(2), 761–768 (2007).
8. A. Sutin, A. Sarvazyan, P. A. Johnson, *et al.*, "Land mine detection by time-reversal acousto-seismic method," J. Acoust. Soc. Am. **115**(5_Supplement), 2384 (2004).
9. G. Lerosey, J. de Rosny, A. Tourin, *et al.*, "Time reversal of electromagnetic waves," Phys. Rev. Lett. **92**(19), 193904 (2004).
10. G. Lerosey, J. de Rosny, A. Tourin, *et al.*, "Time Reversal of Wideband Microwaves," Appl. Phys. Lett. **88**(15), 154101 (2006).
11. L. Bellomo, S. Pioch, M. Saillard, *et al.*, "Time reversal experiments in the microwave range: description of the radar and results," Progress in Electromag. Res. **104**, 427–448 (2010).
12. Y. Chen, F. Han, Y.-H. Yang, *et al.*, "Time-reversal wireless paradigm for green internet of things: An Overview," IEEE Internet Things J. **1**(1), 81–98 (2014).
13. G. C. Alexandropoulos, A. Mokh, R. Khayatzadeh, *et al.*, "Time Reversal for 6G Spatiotemporal Focusing: Recent Experiments, Opportunities, and Challenges," IEEE Veh. Technol. Mag. **17**(4), 74–82 (2022).
14. J. D. Schwartz, J. Azaña, and D. V. Plant, "An electronic temporal imaging system for compression and reversal of arbitrary UWB waveforms," *2008 IEEE Radio and Wireless Symposium*, Orlando, FL, USA, 2008.
15. R. Salem, M. A. Foster, and A. L. Gaeta, "Application of space-time duality to ultrahigh-speed optical signal processing," Adv. Opt. Photonics **5**(3), 274–317 (2013).
16. F. Coppinger, A. S. Bhushan, and B. Jalali, "Time reversal of broadband microwave signals," Electron. Lett. **35**(15), 1230–1232 (1999).
17. B. Li and J. Azaña, "Incoherent-light temporal stretching of high-speed intensity waveforms," Opt. Lett. **39**(14), 4243–4246 (2014).
18. J. Zhang and J. Yao, "Broadband and Precise Microwave Time Reversal Using a Single Linearly Chirped Fiber Bragg Grating," IEEE Trans. Microwave Theory Tech. **63**(7), 2166–2172 (2015).
19. X. Xie, G. Chen, F. Yin, *et al.*, "Time reversal of broadband microwave signal based on frequency conversion of multiple subbands," Opt. Lett. **48**(8), 2110–2113 (2023).
20. H. Linget, L. Morvan, J.-L. Le Gouet, *et al.*, "Time reversal of optically carried radiofrequency signals in the microsecond range," Opt. Lett. **38**(5), 643–645 (2013).
21. A. Louchet-Chauvet, "Analog time-reversal of optically-carried RF signals with a rare earth ion-doped processor with broadband potential," *International Topical Meeting on Microwave Photonics (MWP)*, Toulouse, France, 2018, pp. 1–4.

Optics EXPRESS

22. T. Llauze and A. Louchet-Chauvet, "Analog phase-sensitive time-reversal of optically-carried radiofrequency signals," arXiv (2025).
23. C. Schnébelin, J. Azaña, and H. Guillet de Chatellus, "Programmable broadband optical field spectral shaping with megahertz resolution using a simple frequency shifting loop," Nat. Commun. **10**(1), 4654 (2019).
24. V. Durán, C. Schnébelin, and H. Guillet de Chatellus, "Coherent multi-heterodyne spectroscopy using acousto-optic frequency combs," Opt. Express **26**(11), 13800–13809 (2018).
25. V. Billault, V. Durán, C. R. Fernández-Pousa, *et al.*, "All-optical coherent pulse compression for dynamic laser ranging using an acousto-optic dual comb," Opt. Express **29**(14), 21369–21385 (2021).
26. L. Alliot de Borggraef and H. Guillet de Chatellus, "Phase-sensitive distributed Rayleigh fiber sensing enabling the real-time monitoring of the refractive index with a sub-cm resolution by all-optical coherent pulse compression," Opt. Express **31**(2), 1167–1180 (2023).
27. H. Guillet de Chatellus, E. Lacot, W. Glastre, *et al.*, "Theory of Talbot lasers," Phys. Rev. A **88**(3), 033828 (2013).
28. H. Guillet de Chatellus, L. Romero Cortés, and J. Azaña, "Optical real-time Fourier transformation with kilohertz resolutions," Optica **3**(1), 1–8 (2016).
29. C. Schnébelin and H. Guillet de Chatellus, "Agile photonic fractional Fourier transformation of optical and RF signals," Optica **4**(8), 907–910 (2017).
30. G. Bourdarot, J.-P. Berger, and H. Guillet de Chatellus, "Multi-delay photonic correlator for wideband RF signal processing," Optica **9**(4), 325–334 (2022).
31. H. Guillet de Chatellus, "Compact real-time RF spectrum analyzer with 16 GHz instantaneous bandwidth based on photonic frequency-shifting loops," Opt. Continuum **2**(6), 1276–1286 (2023).
32. V. Durán, L. Djevarhidjian, and H. Guillet de Chatellus, "Bidirectional frequency-shifting loop for dual-comb spectroscopy," Opt. Lett. **44**(15), 3789–3792 (2019).
33. V. Billault, V. Crozatier, G. Baili, *et al.*, "Dynamic behavior of frequency combs in frequency-shifting loops," J. Opt. Soc. Am. B **37**(6), 1812–1820 (2020).
34. N. Kanagaraj, L. Djevarhidjian, V. Durán, *et al.*, "Optimization of acousto-optic optical frequency combs," Opt. Express **27**(10), 14842–14852 (2019).
35. C. Fernández-Pousa and H. Guillet de Chatellus, "Fundamental SNR limits imposed by ASE in frequency-shifting loops," J. Lightwave Technol. **40**(20), 6831–6844 (2022).